

Giulio Ventura  
Elena Benvenuti *Editors*

# Advances in Discretization Methods

Discontinuities, Virtual Elements,  
Fictitious Domain Methods

# SEMA SIMAI Springer Series

---

Series Editors: Luca Formaggia • Pablo Pedregal (Editors-in-Chief)  
Jean-Frédéric Gerbeau • Tere Martinez-Seara Alonso • Carlos Parés • Lorenzo Pareschi •  
Andrea Tosin • Elena Vazquez • Jorge P. Zubelli • Paolo Zunino

---

Volume 12

More information about this series at <http://www.springer.com/series/10532>

Giulio Ventura • Elena Benvenuti

Editors

# Advances in Discretization Methods

Discontinuities, Virtual Elements, Fictitious  
Domain Methods



Springer

*Editors*

Giulio Ventura  
Structural, Building, Geotechnical Eng.  
Politecnico di Torino  
Torino, Italy

Elena Benvenuti  
Department of Engineering  
University of Ferrara  
Ferrara, Italy

ISSN 2199-3041

SEMA SIMAI Springer Series

ISBN 978-3-319-41245-0

DOI 10.1007/978-3-319-41246-7

ISSN 2199-305X (electronic)

ISBN 978-3-319-41246-7 (eBook)

Library of Congress Control Number: 2016950209

© Springer International Publishing Switzerland 2016

This work is subject to copyright. All rights are reserved by the Publisher, whether the whole or part of the material is concerned, specifically the rights of translation, reprinting, reuse of illustrations, recitation, broadcasting, reproduction on microfilms or in any other physical way, and transmission or information storage and retrieval, electronic adaptation, computer software, or by similar or dissimilar methodology now known or hereafter developed.

The use of general descriptive names, registered names, trademarks, service marks, etc. in this publication does not imply, even in the absence of a specific statement, that such names are exempt from the relevant protective laws and regulations and therefore free for general use.

The publisher, the authors and the editors are safe to assume that the advice and information in this book are believed to be true and accurate at the date of publication. Neither the publisher nor the authors or the editors give a warranty, express or implied, with respect to the material contained herein or for any errors or omissions that may have been made.

Printed on acid-free paper

This Springer imprint is published by Springer Nature  
The registered company is Springer International Publishing AG Switzerland

# Preface

This volume of the SEMA SIMAI Springer Series brings together selected contributions presented at the international conference “eXtended Discretization MethodS” (X-DMS), held during September 2015 in Ferrara, Italy. The conference was one of the thematic conferences supported by the European Community in Computational Methods in Applied Sciences (ECCOMAS) and also one of the special interest conferences sponsored by the International Association for Computational Mechanics (IACM). Twelve minisymposia, more than one hundred oral presentations, and plenary lectures given by eminent personalities in the computational mechanics research field contributed to the scientific value of the event.

In gathering some of the most interesting contributions at the X-DMS 2015 Conference, the book aims to disseminate ideas and to promote discussion among researchers with an interest in the development and application of computational methods in science and technology. In line with this objective, the volume addresses some of the most advanced discretization methods for the numerical analysis of a variety of physical problems. In recent years, the efforts of the scientific community in computational mechanics have especially focused on improving both the overall computational efficiency and the versatility of the methods, including the addition of special features of the solution directly in the approximation and/or discretization space. The results of these efforts can be found in a wide range of computational methodologies, including partition of unity finite element methods (meshfree, XFEM, GFEM), virtual element and fictitious domain methods, special techniques for static and evolving interfaces, multiscale discretization, strong discontinuity approaches. The selected contributions in this volume recall the main aspects of some of these methodologies, demonstrating their potentialities and possibilities for application.

The book is organized into four parts. Part I focuses on the proposals of numerical schemes for simulations in porous and fractured media; here the challenge is to handle effectively complex geometries coupled with complex physical problems. Part II deals with some of the most advanced recent techniques, based on hybrid and extended discretization methods, for fracture and interface problems. Evolving fractures in polycrystalline materials, crack lip contact modelling, and procedures

for the computation of stress intensity factors are some of the addressed topics. Part **III** is devoted to contributions on polygonal and polyhedral methods: these methods consist in using general polytopes, as opposed to more standard tetrahedra and hexahedra, for the discretization of partial differential equations. Specialized forms of the discontinuous Galerkin method and the virtual element method represent the core of this section. In Part **IV**, recent advances involving extended finite element methods and fictitious domain methods are introduced; the goals are especially to overcome some fundamental problems relating to these methods, which are basically integration at the element level and ill-conditioning of the resulting system of equations.

A common feature of all the selected contributions is the direct link between computational methodologies and their application to different engineering topics. This mix of theory and application reveals an underlying cooperation between mathematicians and engineers and highlights the way in which the scientific world is reacting to the increasing demand for simulations to contribute to the development of sustainable future technologies in engineering, biomedicine, and environmental sciences.

The Editors of this volume wish to express their sincere gratitude to all the actors involved in the X-DMS 2015 Conference, from the Institutions and Sponsors to the Scientific Committee, the organizers of the minisymposia, the plenary speakers, and all the participants.

Finally, special acknowledgments are due to Prof. Luca Formaggia, Editor-in-Chief of the SEMA SIMAI Springer Series, and to the Springer Milan editorial office for offering the opportunity to compile this volume.

Torino, Italy  
Ferrara, Italy  
May 2016

Giulio Ventura  
Elena Benvenuti

# Contents

<b>Part I   Enriched Methods for Flow and Mechanics in Heterogeneous Media</b>	
<b>A Mixed Finite Element Method for Modeling the Fluid Exchange Between Microcirculation and Tissue Interstitium .....</b>	<b>3</b>
Domenico Notaro, Laura Cattaneo, Luca Formaggia, Anna Scotti, and Paolo Zunino	
<b>On a PDE-Constrained Optimization Approach for Flow Simulations in Fractured Media.....</b>	<b>27</b>
Sandra Pieraccini and Stefano Scialò	
<b>A Review of the XFEM-Based Approximation of Flow in Fractured Porous Media .....</b>	<b>47</b>
Bernd Flemisch, Alessio Fumagalli, and Anna Scotti	
<b>Part II   Enhanced Finite Element Formulations for Fracture and Interface Problems</b>	
<b>Modeling of Fracture in Polycrystalline Materials .....</b>	<b>79</b>
Steffen Beese, Stefan Loehnert, and Peter Wriggers	
<b>eXtended Hybridizable Discontinuous Galerkin (X-HDG) for Void and Bimaterial Problems .....</b>	<b>103</b>
Ceren Gürkan, Esther Sala-Lardies, Martin Kronbichler, and Sonia Fernández-Méndez	
<b>Crack Lip Contact Modeling Based on Lagrangian Multipliers with X-FEM.....</b>	<b>123</b>
Yuan Jin, Olivier Pierard, Eric Wyart, and Eric Béchet	
<b>Stress Intensity Factors Through Crack Opening Displacements in the XFEM .....</b>	<b>143</b>
Markus Schätzer and Thomas-Peter Fries	



### **Part III Polygonal and Polyhedral Methods**

<b>The Virtual Element Method for Underground Flow Simulations in Fractured Media</b> .....	167
Matías Fernando Benedetto, Stefano Berrone, and Andrea Borio	
<b>Adaptive Discontinuous Galerkin Methods on Polytopic Meshes</b> .....	187
Joe Collis and Paul Houston	

### **Part IV Advances in XFEM/Fictitious Domain Methods**

<b>Stabilized X-FEM for Heaviside and Nonlinear Enrichments</b> .....	209
Giulio Ventura and Claudia Tesei	
<b>An Adaptive Fictitious Domain Method for Elliptic Problems</b> .....	229
Stefano Berrone, Andrea Bonito, and Marco Verani	
<b>Higher-Order Accurate Integration for Cut Elements with Chen-Babuška Nodes</b> .....	245
Thomas-Peter Fries	

**Part I**  
**Enriched Methods for Flow and Mechanics**  
**in Heterogeneous Media**

# A Mixed Finite Element Method for Modeling the Fluid Exchange Between Microcirculation and Tissue Interstitium

Domenico Notaro, Laura Cattaneo, Luca Formaggia, Anna Scotti,  
and Paolo Zunino

**Abstract** Thanks to dimensional (or topological) model reduction techniques, small inclusions in a three-dimensional (3D) continuum can be described as one-dimensional (1D) concentrated sources, in order to reduce the computational cost of simulations. However, concentrated sources lead to singular solutions that still require computationally expensive graded meshes to guarantee accurate approximation. The main computational barrier consists in the ill-posedness of restriction operators (such as the trace operator) applied on manifolds with co-dimension larger than one. We overcome the computational challenges of approximating PDEs on manifolds with high dimensionality gap by means of nonlocal restriction operators that combine standard traces with mean values of the solution on low dimensional manifolds. This new approach has the fundamental advantage of enabling the approximation of the problem using Galerkin projections on Hilbert spaces, which could not be otherwise applied because of regularity issues. This approach, previously applied to second order PDEs, is extended here to the mixed formulation of flow problems with applications to microcirculation. In this way we calculate, in the bulk and on the 1D manifold simultaneously, the approximation of velocity and pressure fields that guarantees good accuracy with respect to mass conservation.

## 1 Introduction

The ultimate objective of the project is to perform large scale simulations of microcirculation. In the context of blood flow, the application of geometrical model reduction techniques plays an essential role, see for example [10, 18]. In particular, small vessels embedded into a continuum can be described as one-dimensional (1D) concentrated sources, in order to reduce the computational cost of simulations.

---

D. Notaro • L. Cattaneo • L. Formaggia • A. Scotti • P. Zunino (✉)  
MOX, Department of Mathematics, Politecnico di Milano, piazza Leonardo da Vinci 32,  
20133 Milano, Italy  
e-mail: [domenico.notaro@mail.polimi.it](mailto:domenico.notaro@mail.polimi.it); [laura1.cattaneo@polimi.it](mailto:laura1.cattaneo@polimi.it); [luca.formaggia@polimi.it](mailto:luca.formaggia@polimi.it);  
[anna.scotti@polimi.it](mailto:anna.scotti@polimi.it); [paolo.zunino@polimi.it](mailto:paolo.zunino@polimi.it)

Although the coupling of three-dimensional (3D) continua with embedded (1D) networks arises in applications of paramount importance such as microcirculation, flow through perforated media and the study of reinforced materials, it has not been well investigated yet.

Two remarkable examples of methods that were previously proposed to overcome the challenges of simulating small objects into a continuum are the *immersed boundary methods* [15, 17, 22] and the *fictitious domain methods* [11, 12, 21]. Although they share some similarities with the approach that we pursue here, they have never been applied for solving coupled partial differential equations on embedded domains.

In the particular case of microcirculation, many ad-hoc approaches have been proposed. Since capillaries can be modelled as long and narrow cylindrical vessels, asymptotic expansions that exploit the large aspect ratio of the channel can be derived to approximate the fluid exchange from one capillary to the surrounding tissue. This idea has been successfully exploited to study the microvascular flow in simple arrays of capillaries [1, 8, 9]. However, vascular networks are characterized by a complex, possibly irregular geometry. The previous semi-analytic methods may be hardly applied to realistic configurations. We believe that numerical methods may override this obstacle. For example, the method of Green's functions, has been extensively applied to the study complex vascular networks of tumors [13, 19, 20].

In this work we aim to move away from ad-hoc approaches and cast the microcirculation problem into a new unified framework to formulate and approximate coupled partial differential equations (PDEs) on manifolds with heterogeneous dimensionality. The main computational barrier consists in the ill-posedness of restriction operators (such as the trace operator) applied on manifolds with co-dimension larger than one. Following the approach introduced in [6, 7, 14], we will overcome the computational challenges of approximating PDEs on manifolds with high dimensionality gap. The main idea consists of introducing nonlocal restriction operators that combine standard traces with mean values of the solution on low dimensional manifolds, in order to couple the problem solution in 3D with the one in 1D. This new approach has the fundamental advantage to enable the approximation of the problem using Galerkin projections on Hilbert spaces, which could not be otherwise applied, because of regularity issues.

Within this general framework, the specific objective of this work is to formulate the microcirculation problem as a system of coupled 1D and 3D partial differential equations governing the flow through the capillary network and the interstitial volume, respectively. In order to obtain a good approximation of pressure and velocity fields, and in particular to satisfy mass conservation, we formulate the problem in mixed form. Then, we derive a discretization method based on mixed finite elements. Before moving forward to address applications of the method to study pathologies related to microcirculation, such as cancer [3, 4, 16], we address here a thorough validation of the solver based on two benchmark problems.

## 2 Model Set Up

We study a mathematical model for fluid transport in a permeable biological tissue perfused by a capillary network. The domain where the model is defined is composed by two parts,  $\Omega$  and  $\Lambda$ , denoting the interstitial volume and the capillary bed respectively. We assume that the capillaries can be described as cylindrical vessels and  $\Lambda$  denotes the centerline of the capillary network. The capillary radius,  $R$ , is for simplicity considered to be constant. We decompose the network  $\Lambda$  into individual branches  $\Lambda_i$ . Branches are parametrized by the arc length  $s_i$ ; a tangent unit vector  $\lambda_i$  is also defined over each branch, defining in this way an arbitrary branch orientation. Differentiation over the branches is defined using the tangent unit vector as  $\partial_{s_i} := \nabla \cdot \lambda_i$  on  $\Lambda_i$ , i.e.  $\partial_{s_i}$  represents the projection of  $\nabla$  along  $\lambda_i$ . The blood flow along each branch is described by Poiseuille's law for conservation of momentum and mass:

$$\mathbf{u}_v^i = -\frac{R^2}{8\mu} \frac{\partial p_{v,i}}{\partial s_i} \lambda_i, \quad -\pi R^2 \frac{\partial \mathbf{u}_v^i}{\partial s_i} = g_i \quad \text{on } \Lambda_i, \quad (1)$$

where  $g_i$  is the transmural flux leaving the vessel. As a consequence of the geometrical assumptions, the vessel velocity has fixed direction and unknown scalar component along the branches, namely  $\mathbf{u}_v^i = u_v^i \lambda_i$ . We shall hence formulate the vessel problem using the scalar unknown  $u_v$ . The governing flow equations for the whole network  $\Lambda$  are obtained by summing (1) over the index  $i$ .

We consider the interstitial volume  $\Omega$  as an isotropic porous medium, described by the Darcy's law, namely

$$\mathbf{u}_t = -\frac{1}{\mu} \mathbb{K} \nabla p_t, \quad (2)$$

where  $\mathbf{u}_t$  is the average velocity vector in the tissue,  $\mathbb{K} = k\mathbb{I}$  is the isotropic permeability tensor,  $\mu$  is the viscosity of the fluid and  $p_t$  is the fluid pressure.

The coupled problem for microcirculation and interstitial flow reads as follows

$$\left\{ \begin{array}{ll} \frac{\mu}{k} \mathbf{u}_t + \nabla p_t = 0 & \text{in } \Omega, \\ \nabla \cdot \mathbf{u}_t - f(p_t, p_v) \delta_\Lambda = 0 & \text{in } \Omega, \\ \frac{8\mu}{R^2} u_v + \frac{\partial p_v}{\partial s} = 0 & \text{in } \Lambda, \\ \frac{\partial u_v}{\partial s} + \frac{1}{\pi R^2} f(p_t, p_v) = 0 & \text{in } \Lambda. \end{array} \right. \quad (3)$$

For brevity, we avoid to number each equation of systems. In the remainder, we will refer to single sub-equations within a system using letter numbering from top

to bottom (which does not explicitly appear in the expression of the equation, this notation will be adopted throughout the entire manuscript), e.g. (3) a to d.

The constitutive law for blood leakage from the capillaries to the tissue is provided by means of Starling's law of filtration,

$$f(p_t, p_v) = 2\pi R L_p (p_v - \bar{p}_t), \quad (4)$$

with

$$\bar{p}_t(s) = \frac{1}{2\pi R} \int_0^{2\pi} p_t(s, \theta) R d\theta. \quad (5)$$

Before proceeding, we write the equations in dimensionless form. We choose length, velocity and pressure as primary variables for the analysis. The corresponding characteristic values are: (1) the average spacing between capillary vessels  $d$ , (2) the average velocity in the capillary bed  $U$ , and (3) the average pressure in the interstitial space  $P$ . The dimensionless groups affecting our equations are:

- $R' = \frac{R}{d}$ , non-dimensional radius;
- $\kappa_t = \frac{k}{\mu} \frac{P}{U d}$ , hydraulic conductivity of the tissue;
- $Q = 2\pi R' L_p \frac{P}{U}$ , hydraulic conductivity of the capillary walls;
- $\kappa_v = \frac{\pi R'^4}{8\mu} \frac{P d}{U}$ , hydraulic conductivity of the capillary bed,

and the corresponding dimensionless equations read as follows

$$\left\{ \begin{array}{ll} \frac{1}{\kappa_t} \mathbf{u}_t + \nabla p_t = 0 & \text{in } \Omega, \\ \nabla \cdot \mathbf{u}_t - Q (p_v - \bar{p}_t) \delta_\Lambda = 0 & \text{in } \Omega, \\ \frac{\pi R'^2}{\kappa_v} u_v + \frac{\partial p_v}{\partial s} = 0 & \text{in } \Lambda, \\ \frac{\partial u_v}{\partial s} + \frac{1}{\pi R'^2} Q (p_v - \bar{p}_t) = 0 & \text{in } \Lambda. \end{array} \right. \quad (6)$$

For simplicity of notation, we used the same symbols for the dimensionless variables, i.e velocities and pressure scaled by  $U$  and  $P$ , respectively.

*Remark 1* Equations (6) b and d, counting from the top, can be combined up to obtain a more meaningful formulation of the mass conservation law, namely

$$\nabla \cdot \mathbf{u}_t + \pi R'^2 \frac{\partial u_v}{\partial s} \delta_\Lambda = 0 \quad \text{in } \Omega, \quad (7)$$

meaning that the total amount of fluid in the domain  $\Omega \cup \Lambda$  must be preserved.

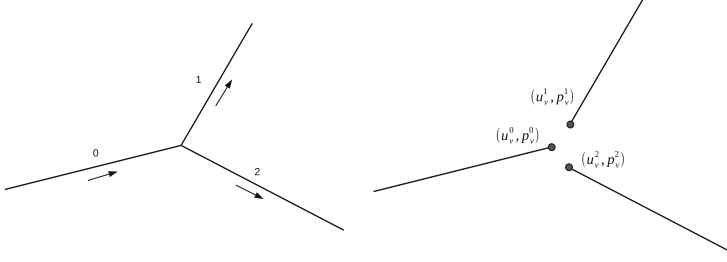


**Fig. 1** On the *left*, a simple network made by a single Y-shaped bifurcation. Arrows show the flow orientation of one inflow branch on the left of the bifurcation point and two outflow branches on the right. On the *right*, the discretization of vessels network is shown. The domain has been split into branches, the flow problem is defined over each branch and compatibility conditions are enforced at the junction point

Boundary conditions will be specified further on for both the tissue and vessel problems. The imposition of suitable compatibility conditions at the bifurcations or branching points of the capillary tree is also necessary to guarantee well posedness of (6). Specifically, we shall enforce conservation of mass and continuity of total pressure at junctions. Let us introduce these conditions in a simple Y-shaped bifurcation network (Fig. 1). Since in the reduced 1D model of the capillary network the cross-section is supposed to be constant over the whole network, the conservation of flow rate is equivalent to require that in correspondence of the junction point  $\mathbf{x}_M$  the inflow velocity  $u_v^0$  is equal the sum of the outflow velocities  $u_v^1, u_v^2$ , namely  $u_v^0(\mathbf{x}_M) = u_v^1(\mathbf{x}_M) + u_v^2(\mathbf{x}_M)$ . Similarly, we require the pressure over each branch to be the same at the junction, namely  $p_v^0(\mathbf{x}_M) = p_v^1(\mathbf{x}_M) = p_v^2(\mathbf{x}_M)$ . The general case of an arbitrary number of *critical* points, possibly with different number of inflow and outflow branches, will be described in Sect. 3. Indeed, it is important to emphasize that such compatibility conditions will be enforced in a natural way, at the level of the variational formulation.

### 3 Variational Formulation

In order to obtain the weak formulation of the tissue interstitium problem, we multiply Eqs. (6) a and b, counting from the top with sufficiently smooth functions and integrate over the volume  $\Omega$ , namely

$$\int_{\Omega} \frac{1}{\kappa_t} \mathbf{u}_t \cdot \mathbf{v}_t \, d\mathbf{x} + \int_{\Omega} \nabla p_t \cdot \mathbf{v}_t \, d\mathbf{x} = 0, \quad (8)$$

$$\int_{\Omega} (\nabla \cdot \mathbf{u}_t) q_t \, d\mathbf{x} - \int_{\Omega} Q(p_v - \bar{p}_t) \delta_{\Lambda} q_t \, d\mathbf{x} = 0. \quad (9)$$

We now apply the Green's theorem to (8) to obtain an anti-symmetric formulation of the Darcy's problem in the tissue:

$$\int_{\Omega} \frac{1}{\kappa_t} \mathbf{u}_t \cdot \mathbf{v}_t \, d\mathbf{x} - \int_{\Omega} p_t (\nabla \cdot \mathbf{v}_t) \, d\mathbf{x} + \int_{\partial\Omega} p_t \mathbf{v}_t \cdot \mathbf{n} \, d\sigma(\mathbf{x}) = 0, \quad (10)$$

$$\int_{\Omega} (\nabla \cdot \mathbf{u}_t) \, q_t \, d\mathbf{x} - \int_{\Omega} Q(p_v - \bar{p}_t) \delta_{\Lambda} q_t \, d\mathbf{x} = 0. \quad (11)$$

As concerns the choice of boundary conditions, for simplicity, we enforce a given pressure distribution over  $\partial\Omega$ , namely

$$p_t = g_t \quad \text{on} \quad \partial\Omega, \quad (12)$$

where  $g_t \in L^2(\partial\Omega)$ . The weak formulation of the problem in  $\Omega$  reads

$$\begin{aligned} \int_{\Omega} \frac{1}{\kappa_t} \mathbf{u}_t \cdot \mathbf{v}_t \, d\mathbf{x} - \int_{\Omega} p_t (\nabla \cdot \mathbf{v}_t) \, d\mathbf{x} &= - \int_{\partial\Omega} g_t \mathbf{v}_t \cdot \mathbf{n} \, d\sigma(\mathbf{x}) \\ \int_{\Omega} (\nabla \cdot \mathbf{u}_t) \, q_t \, d\mathbf{x} - \int_{\Omega} Q(p_v - \bar{p}_t) \delta_{\Lambda} q_t \, d\mathbf{x} &= 0 \end{aligned}$$

For the vessel problem we start giving a general functional framework. At this point, we only require regularity for vessel velocity and pressure over each branch separately:

$$V_v = \bigcup_{i=1}^N H^1(\Lambda_i) \quad Q_v = \bigcup_{i=1}^N L^2(\Lambda_i).$$

The definition of trial and test spaces will be revised in the sequel, in the light of the particular junction conditions we will chose, while no boundary conditions are enforced in the definition of the spaces. As for the tissue problem, we multiply Eqs. (6.c),(6.d) by sufficiently smooth test functions and integrate over  $\Lambda$ :

$$\int_{\Lambda} \frac{\pi R'^2}{\kappa_v} u_v v_v \, ds + \int_{\Lambda} \frac{\partial p_v}{\partial s} v_v \, ds = 0, \quad (13)$$

$$\int_{\Lambda} \frac{\partial u_v}{\partial s} q_v \, ds + \frac{1}{\pi R'^2} \int_{\Lambda} Q(p_v - \bar{p}_t) q_v \, ds = 0. \quad (14)$$

The integration by parts is not trivial in this case because the vessel variables  $p_v$  and  $u_v$  may be discontinuous at multiple junctions. Let us treat separately the second integral of (13) and decompose it over the individual branches  $\Lambda_i$ :

$$\int_{\Lambda} \frac{\partial p_v}{\partial s} v_v \, ds = \sum_{i=1}^N \int_{\Lambda_i} \frac{\partial p_v}{\partial s} v_v \, ds = - \int_{\Lambda} p_v \frac{\partial v_v}{\partial s} \, ds + \sum_{i=1}^N [p_v v_v]_{\Lambda_i^-}^{\Lambda_i^+}, \quad (15)$$



where  $\Lambda_i^-$  and  $\Lambda_i^+$  represent the inflow and outflow boundaries of  $\Lambda_i$ , according to the orientation  $\lambda_i$ . Let us define the set of the indexes of junction points:

$$\mathcal{J} := \{j \in \mathbb{N} : s_j \in \Lambda, \#(P_{s_j}) \geq 2\},$$

where  $P_{s_j}$  is the *patch* of the  $j$ -th junction node, i.e. the collection of all branches joining at the node, and  $\#$  indicates the counting measure. We also need the following disjoint partition of the indexes in  $P_{s_j}$ . According to the orientation unit vector  $\lambda_i$ , for any branching point  $s_j$  we distinguish branches that are entering the node, whose contribution to mass conservation is positive, from branches who are leaving the node, whose contribution is negative. The former are branches whose outflow region coincides with the point  $s_j$ , while for the latter it is the inflow region:

$$\mathcal{P}_j^{out} := \{i \in \{1, \dots, N\} : \Lambda_i^+ \equiv \{s_j\}\},$$

$$\mathcal{P}_j^{in} := \{i \in \{1, \dots, N\} : \Lambda_i^- \equiv \{s_j\}\},$$

for all  $j \in \mathcal{J}$ . At this point, the fluid mass conservation at each node can be expressed as follows

$$\sum_{i \in \mathcal{P}_j^{out}} u_v|_{\Lambda_i^+} - \sum_{i \in \mathcal{P}_j^{in}} u_v|_{\Lambda_i^-} = 0, \quad \forall j \in \mathcal{J}, \quad (16)$$

where  $\Lambda^{in}, \Lambda^{out}$  indicate the collection of inflow and outflow boundaries of the vessel network, i.e. non junction points where the tangent unit vector is inward-pointing and outward-pointing, respectively. This collection contains the boundary points, i.e. the extrema that also belong to  $\partial\Omega$ , but the inclusion may be strict. However, in this contribution we do not address the issue of network extrema belonging to  $\mathring{\Omega}$ , i.e. we do not consider immersed tips.

In order to enforce such conditions, we proceed as follows. First, we reformulate the last term in (15) by isolating the terms relative to inflow junction nodes from those relative to outflow nodes, namely

$$\sum_{i=1}^N [p_v v_v]_{\Lambda_i^+}^{\Lambda_i^+} = \sum_{j \in \mathcal{J}} \left[ \sum_{i \in \mathcal{P}_j^{out}} p_v v_v|_{\Lambda_i^+} - \sum_{i \in \mathcal{P}_j^{in}} p_v v_v|_{\Lambda_i^-} \right] + [p_v v_v]_{\Lambda^{out}}^{\Lambda^{out}}.$$

Here, we have implicitly assumed the trace of  $(p_v v_v)$  over  $\Lambda_i$  exists for  $v_v$  smooth enough, i.e. the evaluation of the product at the extrema of  $\Lambda_i$  makes sense. Furthermore, we write  $(p_v v_v)(s_j) = p_v(s_j) v_v(s_j)$  for some point  $s_j \in \Lambda$ . This is feasible if the trace of the pressure exists. Obviously, a general  $L^2$  function is not sufficient, the natural choice is  $p_v \in \mathcal{C}^0(\bar{\Lambda})$ , that in particular implies compatibility of pressure values at the junctions. Indeed, if the pressure is continuous at the

junction, we have

$$p_v|_{\Lambda_i^-} \equiv p_v(s_j) \equiv p_v|_{\Lambda_k^+} \quad \forall i \in \mathcal{P}_j^{in}, k \in \mathcal{P}_j^{out} \quad \forall j \in \mathcal{J}. \quad (17)$$

Under that hypothesis, we finally factorize out the pressure and isolate a term that corresponds to the junction conditions for the velocity test functions, that is

$$\sum_{j \in \mathcal{J}} p_v(s_j) \left[ \sum_{i \in \mathcal{P}_j^{out}} v_v|_{\Lambda_i^+} - \sum_{i \in \mathcal{P}_j^{in}} v_v|_{\Lambda_i^-} \right].$$

Then, we weakly enforce mass conservation into the variational formulation by multiplying (16) by the pressure test functions  $q_v$ , which act as a Lagrange multiplier for this constraint, namely

$$\sum_{j \in \mathcal{J}} q_v(s_j) \left[ \sum_{i \in \mathcal{P}_j^{out}} u_v|_{\Lambda_i^+} - \sum_{i \in \mathcal{P}_j^{in}} u_v|_{\Lambda_i^-} \right].$$

Finally, after adding the previous term to Eq. (14), the weak formulation of the vessel problem reads

$$\begin{aligned} \int_{\Lambda} \frac{\pi R^2}{\kappa_v} u_v v_v ds - \int_{\Lambda} p_v \frac{\partial v_v}{\partial s} ds + [p_v v_v]_{\Lambda^{out}} \\ + \sum_{j \in \mathcal{J}} p_v(s_j) \left[ \sum_{i \in \mathcal{P}_j^{out}} v_v|_{\Lambda_i^+} - \sum_{i \in \mathcal{P}_j^{in}} v_v|_{\Lambda_i^-} \right] = 0, \end{aligned} \quad (18)$$

$$\begin{aligned} \int_{\Lambda} \frac{\partial u_v}{\partial s} q_v ds + \frac{1}{\pi R^2} \int_{\Lambda} Q(p_v - \bar{p}_t) q_v ds \\ - \sum_{j \in \mathcal{J}} q_v(s_j) \left[ \sum_{i \in \mathcal{P}_j^{out}} u_v|_{\Lambda_i^+} - \sum_{i \in \mathcal{P}_j^{in}} u_v|_{\Lambda_i^-} \right] = 0. \end{aligned} \quad (19)$$

Concerning the boundary conditions for the vessels network, the natural choice is to enforce a given pressure distributions at the inflow and the outflow of the network,  $p_v = g_v$  on  $\Lambda^{in} \cup \Lambda^{out}$ . The generic regularity requirements for the Dirichlet's datum are measurability and square-summability, namely  $g_v \in L^2(\Lambda^{in} \cup \Lambda^{out})$ . In practice, we consider a constant pressure drop  $\Delta P_v = P_v^{out} - P_v^{in}$ :

$$g_v(s) = \begin{cases} P_v^{in} & s \in \Lambda^{in} \\ P_v^{out} & s \in \Lambda^{out}. \end{cases} \quad (20)$$

Since we are considering the mixed formulation of the problem, we enforce such condition in a weak *natural* way.

At this point, we combine (10), (11), (18), (19) to obtain the whole weak formulation of our 3D-1D coupled model of fluid exchange between microcirculation and tissue interstitium. The variational formulation of problem (6) consists of finding  $\mathbf{u}_t \in \mathbf{V}_t$ ,  $p_t \in Q_t$ ,  $u_v \in V_v$ ,  $p_v \in Q_v$  s.t.

$$\left\{ \begin{array}{ll} \frac{1}{\kappa_t} (\mathbf{u}_t, \mathbf{v}_t)_\Omega - (p_t, \nabla \cdot \mathbf{v}_t)_\Omega = - (g_t, \mathbf{v}_t \cdot \mathbf{n})_{\partial\Omega} & \forall \mathbf{v}_t \in \mathbf{V}_t, \\ (\nabla \cdot \mathbf{u}_t, q_t)_\Omega - Q((p_v - \bar{p}_t) \delta_\Lambda, q_t)_\Omega = 0 & \forall q_t \in Q_t, \\ \frac{\pi R'^2}{\kappa_v} (u_v, v_v)_\Lambda - (p_v, \partial_s v_v)_\Lambda \\ \quad + \sum_j p_v(s_j) \left[ \sum_i v_v|_{\Lambda_i^+} - \sum_i v_v|_{\Lambda_i^-} \right] = - [g_v v_v]_{\Lambda_{in}}^{\Lambda_{out}} & \forall v_v \in V_v, \\ (\partial_s u_v, q_v)_\Lambda + \frac{1}{\pi R'^2} Q(p_v - \bar{p}_t, q_v)_\Lambda \\ \quad - \sum_j q_v(s_j) \left[ \sum_i u_v|_{\Lambda_i^+} - \sum_i u_v|_{\Lambda_i^-} \right] = 0 & \forall q_v \in Q_v. \end{array} \right. \quad (21)$$

## 4 Numerical Approximation

The discretization of problem (6) is achieved by means of the finite element method that arises from the variational formulation (21) combined with a discretization of the domain. In particular, one of the advantage of our formulation is that the partitions of  $\Omega$  and  $\Lambda$  are completely independent. Let us now analyze the two approximations separately.

We denote with  $\mathcal{T}_t^h$  an admissible family of partitions of  $\bar{\Omega}$  into tetrahedrons  $K$

$$\bar{\Omega} = \bigcup_{K \in \mathcal{T}_t^h} K,$$

that satisfies the usual conditions of a conforming triangulation of  $\Omega$ . Here,  $h$  denotes the mesh characteristic size, i.e.  $h = \max_{K \in \mathcal{T}_t^h} k_K$ , being  $k_K$  the diameter of simplex  $K$ . Moreover, we are implicitly assuming that  $\Omega$  is a *polygonal* domain. The solutions of (21) a and b, counting from the top are approximated using discontinuous piecewise-polynomial finite elements for pressure and

$\mathbf{H}^{div}$ -conforming *Raviart-Thomas* finite elements [2] for velocity, namely

$$\mathbb{Y}_h^k := \{ w_h \in L^2(\Omega) : w_h|_K \in \mathcal{P}_{k-1}(K) \quad \forall K \in \mathcal{T}_t^h \},$$

$$\mathbb{RT}_h^k := \{ \mathbf{w}_h \in \mathbf{H}((div, \Omega) : \mathbf{w}_h|_K \in \mathcal{P}_{k-1}(K; \mathbb{R}^d) \oplus \mathbf{x} \mathcal{P}_{k-1}(K) \quad \forall K \in \mathcal{T}_t^h \},$$

for every integer  $k \geq 0$ , where  $\mathcal{P}_k$  indicates the standard space of polynomials of degree  $\leq k$  in the variables  $\mathbf{x} = (x_1, \dots, x_d)$ . For the simulations presented later on, the lowest order *Raviart-Thomas* approximation has been adopted, corresponding to  $k = 1$  above. In numerical experiments performed on the 3D problem alone (the test case is not reported here), we have observed quadratic convergence of the pressure field and linear convergence of the velocity field.

Concerning the capillary network, we adopt the same domain splitting technique described at the continuous level, obtaining the following discrete domain:

$$\Lambda_h = \bigcup_{i=1}^N \Lambda_i^h,$$

where  $\Lambda_i^h$  is a finite element mesh on the one-dimensional manifold  $\Lambda_i$ , i.e. a partition of the  $i$ -th network branch made by a sufficiently large number of segments.

The solution of sub-equations (21) c and (21) d, counting from the top, over a given branch  $\Lambda_i$  is approximated using continuous piecewise-polynomial finite element spaces for both pressure and velocity. Since we want the vessel velocity to be discontinuous at multiple junctions, we define the related finite element space over the whole network as the collection of the local spaces of the single branches. Conversely, the pressure has been assumed to be continuous over the network. We will use the following families of finite element spaces for pressure and velocity, respectively:

$$\mathbb{X}_h^{k+1}(\Lambda) := \{ w_h \in \mathcal{C}^0(\bar{\Lambda}) : w_h|_S \in \mathcal{P}_k(S) \quad \forall S \in \Lambda^h \},$$

$$\mathbb{W}_h^{k+2}(\Lambda) := \bigcup_{i=1}^N \mathbb{X}_h^{k+1}(\Lambda_i),$$

for every integer  $k \geq 0$ . As a result, we use generalized Taylor-Hood elements on each network branch, satisfying in this way the local stability of the mixed finite element pair for the network. At the same time, we guarantee that the pressure approximation is continuous over the entire network  $\Lambda$ . In particular, for the numerical experiments shown later on we have used the lowest order, that is  $k = 1$ .

The discrete formulation arising from (21) is hence easily obtained by adding the subscript  $h$  to the weak continuous formulation: find  $\mathbf{u}_{t,h} \in \mathbf{V}_t^h$ ,  $p_{t,h} \in Q_t^h$ ,  $u_{v,h} \in V_v^h$ ,  $p_{v,h} \in Q_v^h$  s.t.

$$\left\{ \begin{array}{l} \frac{1}{\kappa_t} (\mathbf{u}_{t,h}, \mathbf{v}_{t,h})_{\Omega} - (p_{t,h}, \nabla \cdot \mathbf{v}_{t,h})_{\Omega} = - (g_{t,h}, \mathbf{v}_{t,h} \cdot \mathbf{n})_{\partial\Omega} \quad \forall \mathbf{v}_{t,h} \in \mathbf{V}_t^h, \\ (\nabla \cdot \mathbf{u}_{t,h}, q_{t,h})_{\Omega} - Q((p_{v,h} - \bar{p}_{t,h}) \delta_{\Lambda}, q_{t,h})_{\Omega} = 0 \quad \forall q_{t,h} \in Q_t^h, \\ \frac{\pi R^2}{\kappa_v} (u_{v,h}, v_{v,h})_{\Lambda} - (p_{v,h}, \partial_s v_{v,h})_{\Lambda} \\ + \sum_j p_{v,h}(s_j) \left[ \sum_i v_{v,h} |_{\Lambda_i^+} - \sum_i v_{v,h} |_{\Lambda_i^-} \right] = - [g_{v,h} v_{v,h}]_{\Lambda^{out}}^{in} \quad \forall v_{v,h} \in V_v^h \\ (\partial_s u_{v,h}, q_{v,h})_{\Lambda} + \frac{1}{\pi R^2} Q(p_{v,h} - \bar{p}_{t,h}, q_{v,h})_{\Lambda} \\ - \sum_j q_{v,h}(s_j) \left[ \sum_i u_{v,h} |_{\Lambda_i^+} - \sum_i u_{v,h} |_{\Lambda_i^-} \right] = 0 \quad \forall q_{v,h} \in Q_v^h, \end{array} \right. \quad (22)$$

where  $g_{t,h}$ ,  $g_{v,h}$  indicate the discrete counterparts of continuous boundary data.

We observe that (22) is a generalized saddle-point problem arising from the combination of local problems with mass conservation constraints (see also (23)), such as the mixed formulation of Darcy equation and the incompressible flow on each network branch with junction conditions. Although, we guarantee local stability of each block, the global well-posedness is still an open problem, which is under investigation.

## 4.1 Algebraic Formulation

Let us now derive the algebraic form of our discrete problem. We define the number of degrees of freedom of our discrete (finite) spaces as:

$$\begin{aligned} N_t^h &:= \dim(\mathbf{V}_t^h), & M_t^h &:= \dim(Q_t^h), \\ N_v^h &:= \dim(V_v^h), & M_v^h &:= \dim(Q_v^h). \end{aligned}$$

We denote with  $\{\boldsymbol{\varphi}_t^i\}_{i=1}^{N_t^h} \times \{\boldsymbol{\psi}_t^i\}_{i=1}^{M_t^h}$  and  $\{\boldsymbol{\varphi}_v^i\}_{i=1}^{N_v^h} \times \{\boldsymbol{\psi}_v^i\}_{i=1}^{M_v^h}$  the finite element basis for  $\mathbf{V}_t^h \times Q_t^h$  and  $V_v^h \times Q_v^h$  respectively. These two sets are completely independent,

since the 3D and 1D meshes do not conform. We set:

$$\begin{aligned} \mathbf{u}_t^h(\mathbf{x}) &= \sum_{j=1}^{N_t^h} U_t^j \boldsymbol{\varphi}_t^j(\mathbf{x}), \quad p_t^h(\mathbf{x}) = \sum_{j=1}^{M_t^h} P_t^j \psi_t^j(\mathbf{x}) \quad \forall \mathbf{x} \in \Omega_t, \\ u_v^h(s) &= \sum_{j=1}^{N_v^h} U_v^j \varphi_v^j(s), \quad p_v^h(s) = \sum_{j=1}^{M_v^h} P_v^j \psi_v^j(s) \quad \forall s \in \Lambda, \end{aligned}$$

being  $\mathbf{U}_t = \{U_t^j\}_{j=1}^{N_t^h}$ ,  $\mathbf{P}_t = \{P_t^j\}_{j=1}^{M_t^h}$ ,  $\mathbf{U}_v = \{U_v^j\}_{j=1}^{N_v^h}$  and  $\mathbf{P}_v = \{P_v^j\}_{j=1}^{M_v^h}$ , the degrees of freedom of the finite element approximation. Then, by replacing the linear combinations within the discrete weak form (22) and using the linearity of the inner product, from (22) we deduce the following linear system:

$$\begin{bmatrix} \mathbb{M}_{tt} & -\mathbb{D}_{tt}^T & \mathbb{O} & \mathbb{O} \\ \mathbb{D}_{tt} & \mathbb{B}_{tt} & \mathbb{O} & -\mathbb{B}_{tv} \\ \mathbb{O} & \mathbb{O} & \mathbb{M}_{vv} & -\mathbb{D}_{vv}^T - \mathbb{J}_{vv}^T \\ \mathbb{O} & -\mathbb{B}_{vt} & \mathbb{D}_{vv} + \mathbb{J}_{vv} & \mathbb{B}_{vv} \end{bmatrix} \begin{bmatrix} \mathbf{U}_t \\ \mathbf{P}_t \\ \mathbf{U}_v \\ \mathbf{P}_v \end{bmatrix} = \begin{bmatrix} \mathbf{F}_t \\ \mathbf{0} \\ \mathbf{F}_v \\ \mathbf{0} \end{bmatrix}. \quad (23)$$

Standard finite element matrices and right hand sides are defined as follows

$$\begin{aligned} [\mathbb{M}_{tt}]_{i,j} &:= \frac{1}{\kappa_t} (\boldsymbol{\varphi}_t^j, \boldsymbol{\varphi}_t^i)_{\Omega} & \mathbb{M}_{tt} &\in \mathbb{R}^{N_t^h \times N_t^h}, \\ [\mathbb{D}_{tt}]_{i,j} &:= (\nabla \cdot \boldsymbol{\varphi}_t^j, \psi_t^i)_{\Omega} & \mathbb{D}_{tt} &\in \mathbb{R}^{N_t^h \times M_t^h}, \\ [\mathbb{D}_{vv}]_{i,j} &:= (\partial_s \varphi_v^j, \psi_v^i)_{\Lambda} & \mathbb{D}_{vv} &\in \mathbb{R}^{N_v^h \times M_v^h}, \\ [\mathbb{M}_{vv}]_{i,j} &:= \pi R'^2 / \kappa_v (\varphi_v^j, \varphi_v^i)_{\Lambda} & \mathbb{M}_{vv} &\in \mathbb{R}^{N_v^h \times N_v^h}, \\ [\mathbf{F}_t]_i &:= -(g_{t,h}, \boldsymbol{\varphi}_t^i \cdot \mathbf{n})_{\partial\Omega} & \mathbf{F}_t &\in \mathbb{R}^{N_t^h}, \\ [\mathbf{F}_v]_i &:= -[g_{v,h} \varphi_v^i]_{\Lambda}^{out} & \mathbf{F}_v &\in \mathbb{R}^{N_v^h}. \end{aligned}$$

For the implementation of exchange matrices, namely  $\mathbb{B}_{tt}, \mathbb{B}_{tv}, \mathbb{B}_{vt}, \mathbb{B}_{vv}$ , we define two discrete operators: the first one extracts the mean value of a generic basis function of  $Q_t^h$ , while the second interpolates between  $Q_t^h$  and  $Q_v^h$ . For every node  $s_k \in \Lambda^h$  we define  $\mathcal{T}_\gamma(s_k)$  as the discretization of the perimeter of the vessel  $\gamma(s_k)$ , see Fig. 2 for an illustration. For simplicity, we assume that  $\gamma(s_k)$  is a circle of radius  $R$  defined on the orthogonal plane to  $\Lambda^h$  at point  $s_k$ . The set of points of  $\mathcal{T}_\gamma(s_k)$  is used to interpolate the basis functions  $\psi_t^i$ . Let us introduce a local discrete interpolation matrix  $\boldsymbol{\Pi}_\gamma(s_k)$  which returns the values of each test function  $\psi_t^i$  on the set of points belonging to  $\mathcal{T}_\gamma(s_k)$ . Then, we consider the average operator

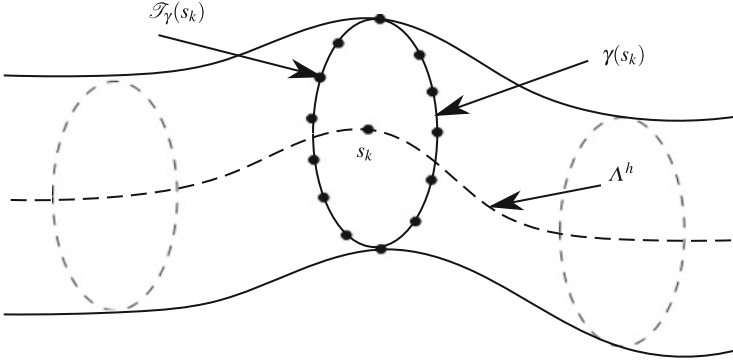


**Fig. 2** Illustration of the vessel with its centerline  $\Lambda^h$ , a cross section, its perimeter  $\gamma(s_k)$  and its discretization  $\mathcal{T}_\gamma(s_k)$  used for the definition of the interface operators  $\bar{\pi}_{vt} : Q_t^h \rightarrow Q_v^h$  and  $\pi_{tv} : Q_v^h \rightarrow Q_t^h$

$\bar{\pi}_{vt} : Q_t^h \rightarrow Q_v^h$  such that  $\bar{q}_t = \bar{\pi}_{vt} q_t$ . The matrix  $\bar{\Pi}_{vt}$  that corresponds to this operator belongs to  $\mathbb{R}^{M_v^h \times M_t^h}$  and it is constructed such that each row is defined as,

$$\bar{\Pi}_{vt}|_k = \mathbf{w}^T(s_k) \Pi_\gamma(s_k) \quad k = 1, \dots, M_v^h \quad (24)$$

where  $\mathbf{w}$  are the weights of the quadrature formula used to approximate the integral

$$\bar{q}_t(s) = \frac{1}{2\pi R} \int_0^{2\pi} q_t(s, \theta) R d\theta$$

on the nodes belonging to  $\mathcal{T}_\gamma(s_k)$ . The discrete interpolation operator  $\pi_{tv} : Q_v^h \rightarrow Q_t^h$  returns the value of each basis function belonging to  $Q_t^h$  in correspondence of nodes of  $Q_v^h$ . In algebraic form it is expressed as an interpolation matrix  $\Pi_{tv} \in \mathbb{R}^{M_v^h \times M_t^h}$ . Using these tools we obtain:

$$\mathbb{B}_{tt} = Q \Pi_{vt}^T \mathbb{M}_{vv}^P \bar{\Pi}_{vt}, \quad (25)$$

$$\mathbb{B}_{tv} = Q \Pi_{vt}^T \mathbb{M}_{vv}^P, \quad (26)$$

$$\mathbb{B}_{vt} = Q/\pi R^2 \mathbb{M}_{vv}^P \bar{\Pi}_{vt}, \quad (27)$$

$$\mathbb{B}_{vv} = Q/\pi R^2 \mathbb{M}_{vv}^P, \quad (28)$$

being  $\mathbb{M}_{vv}^P$  the pressure mass matrix for the vessel problem defined by

$$[\mathbb{M}_{vv}^P]_{i,j} := (\psi_v^j, \psi_v^i)_\Lambda.$$

Concerning the implementation of junction compatibility conditions, we introduce a linear operator giving the restriction with sign of a basis function of  $V_v^h$  over

a given junction node. For a given  $k \in \mathcal{J}$ , we define  $\mathcal{R}_k : V_v^h \rightarrow \mathbb{R}$  such that:

$$\mathcal{R}_k(\varphi_v^j) := \begin{cases} +\varphi_v^j(s_k) & j \text{ in } \Lambda_l^h \wedge l \in \mathcal{P}_k^{out} \\ -\varphi_v^j(s_k) & j \text{ in } \Lambda_l^h \wedge l \in \mathcal{P}_k^{in} \end{cases} \quad (29)$$

for all  $j = 1, \dots, N_v^h$ , where the expression “ $j$  in  $\Lambda_l^h$ ” means that the  $j$ -th dof is linked to some vertex of the  $l$ -th branch. Note that we are implicitly using the usual property of Lagrangian finite element basis functions, i.e. that they vanish on all nodes except the related one. As a consequence, our definition is consistent for all junction vertexes. Indeed,  $\mathcal{R}_k$  may only assume values  $-1, 0, +1$  and in particular  $\mathcal{R}_k(\varphi_v^j) = 0$  for all couples of indexes  $(k, j)$  that are uncorrelated. Furthermore, the definition of  $\mathcal{R}_k$  can be trivially extended to all network vertexes. Using this operator, the generic  $(i, j)$  element of  $\mathbb{J}_{vv}$  may be computed as follows

$$[\mathbb{J}_{vv}]_{i,j} = - \sum_{k \in \mathcal{J}} \mathcal{R}_k(\varphi_v^j) \psi_v^i(s_k). \quad (30)$$

## 5 Numerical Experiments

We validate the mixed-finite element solver through the following test cases, illustrated in Fig. 3, which have been designed to obtain sufficient generality with a straightforward interpretation of the results:

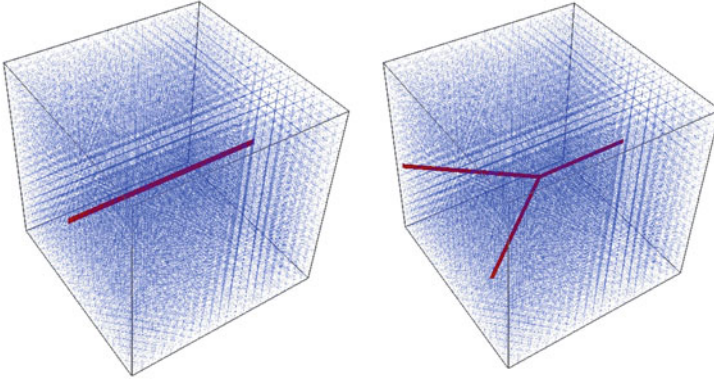


**Fig. 3** (*Left*) Computational domain for test-case I. The discrete network  $\Lambda_h$  is made by a single capillary vessel immersed in a unitary slab of tissue interstitium,  $\Omega_h$ . We have used a discretization step  $h = 0.05$  for both the 1D and 3D problems. (*Right*) Computational domain for test-case II. The discrete vessels network  $\Lambda_h$  is made by three capillaries joined junction point  $\mathbf{x}_M = (0.5, 0.5, 0.5)$ :  $\Lambda_h^0$  entering branch,  $\Lambda_h^1$  and  $\Lambda_h^2$  exiting branches. The tissue interstitium domain  $\Omega_h$  is a unit cube. Again, we have used a discretization step  $h = 0.05$  for both the 1D and 3D problems



- (1) Coupled 3D-1D problem on a single branch;
- (2) Coupled 3D-1D problem on a Y-shaped bifurcation.

In this way, we address the two main modeling issues: (1) first, we test the ability of the computational model to approximate the coupling between 3D and 1D equations; (2) second, we verify that the assembly of junction conditions works properly.

### 5.1 Coupled 3D-1D Problem on a Single Branch

For such a simple setting, we can easily isolate the exchange terms. The 3D-1D coupled problem is given by (6). In this case, the integration by parts in (6)(iii) is standard since there are not any junction points. As a consequence, we replace condition (15) with the following:

$$\begin{aligned} \int_A \frac{\partial p_v}{\partial s} v_v ds &= - \int_A p_v \frac{\partial v_v}{\partial s} ds + [p_v v_v]_{\Lambda^{in}}^{\Lambda^{out}} \\ &= - \int_0^1 p_v \frac{\partial v_v}{\partial s} ds + p_v(1) v_v(1) - p_v(0) v_v(0) \quad . \end{aligned}$$

Therefore, we obtain the following linear system:

$$\begin{bmatrix} \mathbb{M}_{tt} & -\mathbb{D}_{tt}^T & \mathbb{O} & \mathbb{O} \\ \mathbb{D}_{tt} & \mathbb{B}_{tt} & \mathbb{O} & -\mathbb{B}_{tv} \\ \mathbb{O} & \mathbb{O} & \mathbb{M}_{vv} & -\mathbb{D}_{vv}^T \\ \mathbb{O} & -\mathbb{B}_{vt} & \mathbb{D}_{vv} & \mathbb{B}_{vv} \end{bmatrix} \begin{bmatrix} \mathbf{U}_t \\ \mathbf{P}_t \\ \mathbf{U}_v \\ \mathbf{P}_v \end{bmatrix} = \begin{bmatrix} \mathbf{F}_t \\ \mathbf{0} \\ \mathbf{F}_v \\ \mathbf{0} \end{bmatrix} . \quad (31)$$

We recall that submatrices in (31) have been defined in Sect.4.1. Nevertheless, according to the above expression of vessel boundary term it is possible to specify the right hand side, namely

$$\mathbf{F}_v = -[g_{v,h} \varphi_v^i]_0^1 \equiv \begin{bmatrix} g_{v,h}(0) \\ 0 \\ \vdots \\ 0 \\ -g_{v,h}(1) \end{bmatrix} \quad (32)$$

being  $g_{v,h}$  the discrete counterpart of the vessel boundary datum. In the last equality we used the fundamental property of finite element basis functions. Note that (31) equals the generic linear system (23) in the special case  $\mathbb{J}_{vv} = \mathbb{O}$ .

### 5.1.1 Numerical Results

For the tissue sample  $\Omega_h$  we use a tetrahedral structured mesh,  $\mathcal{T}_h$ , with characteristic size  $h = 1/20$ ; the same step has been used for the network discretization  $\Lambda_h$ , resulting in 48,000 elements for the approximation of interstitial volume and 60 elements for the discrete network. We prescribe the following boundary conditions:

$$p_t|_{\partial\Omega} = 0, \quad p_v(0) = 1.0, \quad p_v(1) = 0.5. \quad (33)$$

For the solution of the linear system (31) we developed a C++ code based on GetFEM++ (see <https://home.gna.org/getfem>), an open-source general purpose finite element library. Specifically, we applied the direct solver *SuperLU* 3.0 (see <http://crd.lbl.gov/verb~xiaoye/SuperLU>). Numerical solutions are shown in Fig. 4. These plots show qualitatively that the definition and implementation of the method works properly. In order to find a *quantitative* way to validate our numerical method we exploit the exact solution proposed by Chapman and Shipley [5] for the single

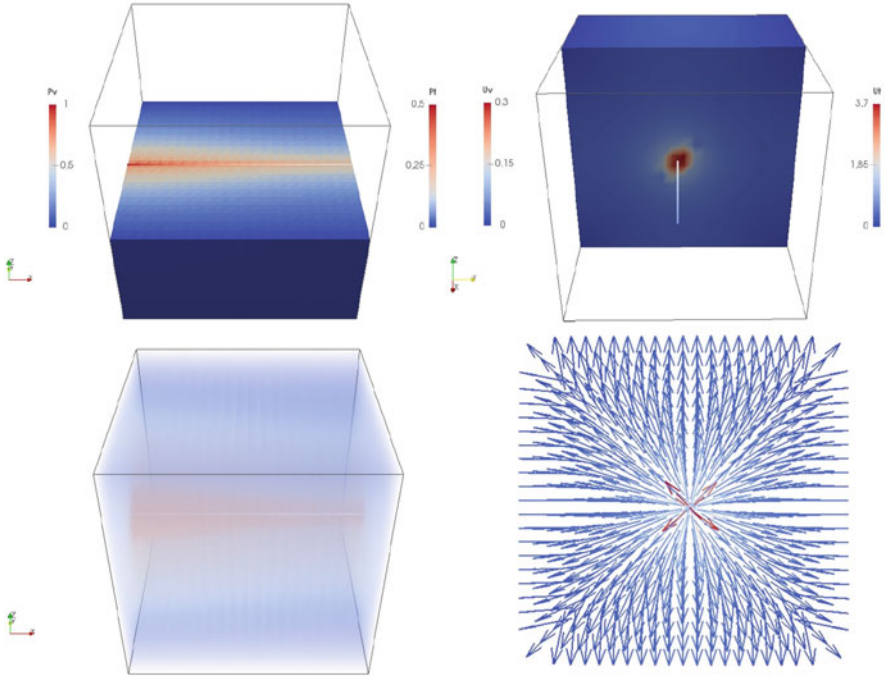


**Fig. 4** Coupling between the vessel and tissue interstitium. Numerical solutions obtained with mesh size  $h = 0.05$  and parameters  $\kappa_t = \kappa_v = 1$ ,  $R' = 1$ ,  $Q = 1$ . On the left a double-check for pressure exchange: (*top-left*) visualization of tissue and vessel pressures at the transversal medium plane, (*bottom-left*) a 3D qualitative representation. On the right the velocity exchange: (*top-right*) visualization of tissue and vessel velocities at the axial medium plane, (*bottom-right*) a 2D view of the vector field

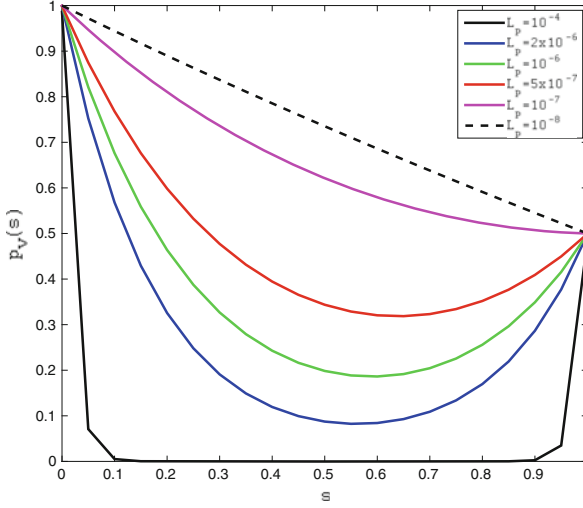


**Fig. 5** Capillary pressure as function of arclength  $s$  for different vascular permeabilities  $\hat{L}_p = 10^{-4}, 2 \times 10^{-6}, 10^{-6}, 5 \times 10^{-7}, 10^{-7}, 10^{-8}$ . To be compared with Fig. 7 in [5]

branch problem. In that work the authors model a fluid flow through the leaky neovasculature and porous interstitium of a solid tumor, in particular they consider the simplest case of an isolated capillary immersed in a tumor tissue, giving rise to the same problem addressed here.

Finally, in order to reproduce numerical results of [5] we choose the non-dimensional parameters of the problem as follows

$$R' = 10^{-2}, \quad \kappa_t = 4, \quad \kappa_v = \pi R'^3 / 8 \hat{L}_p, \quad Q = 2\pi, \quad (34)$$

where  $\hat{L}_p \in \{10^{-4}, 2 \times 10^{-6}, 10^{-6}, 5 \times 10^{-7}, 10^{-7}, 10^{-8}\}$  is an array of non-dimensional vascular permeabilities used in the numerical tests of [5]. In Fig. 5 we represent the capillary pressure as a function of arc-length for different vascular permeabilities. We can observe perfect agreement with the plots shown in [5] (not reported here). Moreover, we notice that for the lowest value of the vascular permeability  $\hat{L}_p$ , corresponding to an almost impermeable vessel, the computational model predicts a linearly decreasing pressure, in agreement with the Poiseuille equation that governs the flow. Conversely, for high permeability values there is a substantial deviation from the linear trend because the leakage dominates over the axial flow component.

In addition, a sensitivity analysis has been performed to investigate the influence of the relative position of the 3D and 1D grids. To this purpose, we simulated three different configurations in which the network vertexes coincide with particular points of the 3D mesh, as shown in Fig. 6. Numerical results of similar test cases, where the 1D mesh is slightly shifted to coincide with the location of Fig. 6 (top),

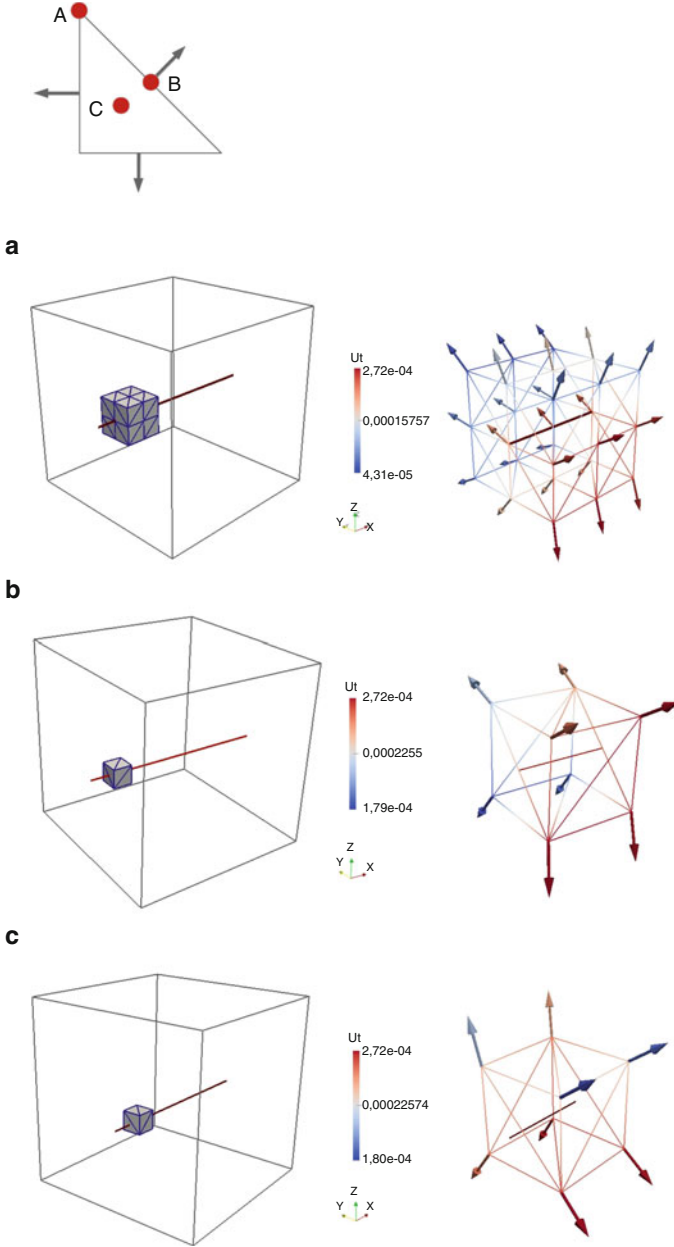


**Fig. 6** (Top panel) Proposed configurations for 1D/3D mesh correlation analysis. The *red dots*  $A, B, C$  indicate three meaningful configurations w.r.t. the distribution of Raviart-Thomas dof (arrows). We show below the sensitivity analysis for the 1D/3D mesh coupling. Numerical solutions have been obtained with mesh size  $h = 0.1$  and parameters  $\kappa_t = \kappa_v = 1$ ,  $R' = 1$ ,  $Q = 10^{-4}$ . For each of the three configurations  $A, B, C$ , we extract the smallest patch of elements intersected by the 1D mesh (truncated along the axial direction for visualization purposes). The *local velocity field* is also displayed together with its magnitude (color scale)